*Article*

# The difference of corrosion behavior in initial period for the hot-rolled and cold-rolled 2205 duplex stainless steel

**Tao Gao, Jian Wang*, Qi Sun, Peide Han***

College of Materials Science and Engineering, Taiyuan University of Technology, 79 Yingze west street, Taiyuan, 030024, China

*Correspondence: wangjian@tyut.edu.cn (J. Wang), hanpeide@tyut.edu.cn (P.D. Han)

**Abstract:** The precipitate phases often play an important influence on the corrosion resistance of 2205 Duplex stainless steel (DSS). In the presented paper, the microstructure and corrosion resistance in the hot-rolled and cold-rolled 2205 DSS aging for different time at 850 °C was investigated by XRD, SEM and potentiodynamic polarization. It has been found that the Chi(χ) phase and Sigm(σ) phase were precipitated in turn after aging treatment of hot-rolled and cold-rolled materials, but the precipitate amount in cold-rolled material is much more than that of hot-rolled samples. The corrosion resistance of the solution-annealed cold-rolled material is similar to the hot-rolled material, but the corrosion resistance of cold-rolled material with precipitate is weaker than that of hot-rolled material after aging treatment. Pitting initiates preferentially in the Cr-depleted region from σ phase in aged hot-rolled 2205, and severe selective corrosion occurs on sigma/ferrite interfaces aged for a long aged lime. However, the initiation of pitting corrosion may take place at the phase boundary, defect and martensite in the aged cold-rolled 2205. The σ phase is further selectively dissolved by electrochemical method to investigate the difference of microstructure and corrosion behavior in hot-rolled and cold-rolled 2205 duplex stainless steel.

**Keywords:** Pitting; Sigma phase; 2205; Duplex stainless steel

## 1. Introduction

The 2205 duplex stainless steels (DSS), with excellent corrosion performance as well as good mechanical property, have been an important class of engineering alloys for many years and provide wide applications in many industrial fields, especially in the aggressive environment [1-6]. The effect of microstructural modifications of 2205 DSS on their mechanical and corrosive behavior was intensively investigated in the past. Few works highlighted the changes of corrosion resistance performances caused by phase proportion of austenite and ferrite[7,8]. Several researches discussed the passive films properties of the 2205 DSS during the electrochmical corrosion[9-12]. Some studies also indicated that the pitting corrosion of 2205 DSS often initiated from the σ phase due to the depletion of Cr and Mo[13,14].

However, due to the high content of alloying elements in 2205 DSS, the secondary phases such as σ, χ, $Cr_2N$, α′ and $M_{23}C_6$ were also easily precipitated between approximately 300~1000℃, leading to a detrimental influence on both mechanical properties and corrosion behavio[15,16]. The χ phase, as a precursor of σ phase, gradually disappear with the precipitation of σ phase. The $M_{23}C_6$ phase usually formed on the austenite grain boundaries during isothermal heating at 950℃. The $Cr_2N$ were often found in ferrite phase after rapid cooling from higher annealing temperature of 1050-1250℃. Compared to these phase, the σ phase was more easily precipitated and had much

more effect on the materials properties[17-19]. Some researchers have focused on the precipitation process of σ phase. Chen et al. found the σ phase was often precipitated at the α/γ interphase boundaries after the sample was aged at 900℃for 5 min[20]. Elmer et al. in situ observed the dissolution of the sigma phase in 2205 duplex stainless steel, and the σ phase can be detected after aging at 850℃only 81s, but completely dissolving with the increase of temperature to 985℃[21]. Sieurin et al. found the sensitive temperature of σ phase in 2205 DSS was between 650 and 920℃, and the "nose temperature" was about 850℃ in TTP (temperature-time-precipitation) diagram[22].

In fact, it is inevitable that some treatments such as welding and other thermal treatments could cause the precipitates in 2205 DSS when it exposed in the sensitive temperature of precipitates[23-25]. The cold rolling is an industrial technique for hardening alloy, it will also produce a large amount of deformation and increase the grain energy, finally affecting the precipitation behavior and microstructure of the materials[26]. Cho et al. has found the cold deformation promote the precipitation of σ phase in 2205 DSS, as compared with the non-cold-rolled materials[27]. Breda et al. revealed the strain-induced martensite occur in the cold-rolled 2205 DSS[28]. However, research about the influence of precipitates on the corrosion behavior of hot-rolled and cold-rolled 2205 DSS has rarely been contrasted so far.

In the present work, the sigma phase induced pitting and selective corrosion in the hot-rolled and cold-rolled 2205 DSS was investigated. The changes of the microstructures and the corrosion resistance of the 2205 DSS with hot-rolled or cold-rolled state aging at 850℃ for different time was studied by X-ray diffraction (XRD), scanning electron microscope (SEM), and potentiodynamic polarization. Besides that, the sample after corrosion tests were collected and characterized to distinguish the corrosion mechanism in hot-rolled and cold-rolled 2205 DSS. The σ phase of the aged sample was also removed by electrochemical-etching method, in order to clarify its effect on the corrosion resistance.

## 2. Materials and Methods

The DSS utilized in this study was typical 2205 that were supplied by the Taiyuan iron&steel company Ltd. (TISCO). The hot-rolled 2205 stainless steels plates with a thickness of 4 mm and cold-rolled 2205 stainless steels plates with a thickness of 2 mm that had been cut into small blocks with a size of 1 cm ×1 cm were first solution-treated at 1323 K for 1 h and then quenched in water to balance of ferrite and austenite. The chemical composition is shown in Table 1. Given the "nose temperature", aging treatments were carried out on the specimens at 850℃for different time ranging from 10 min to 4 h. Afterwards, each specimen was mounted in epoxy resin, mechanically ground with SiC papers down to 3000 grit, polished to mirror finish, and subsequently cleaned through employing distilled water and ethanol.

**Table 1** Chemical composition of 2205 duplex stainless steel (wt. %)

| Cr | Ni | Mo | Mn | Si | N | P | S | C | Fe |
|---|---|---|---|---|---|---|---|---|---|
| 22.36 | 5.21 | 3.18 | 1.37 | 0.65 | 0.15 | 0.014 | 0.0008 | 0.020 | Bal. |

Prior to use, all samples were etched using a mixed solution with the $K_2S_2O_5$ (0.3 g), HCl (20 mL) and $H_2O$ (80 mL). The microstructures of sample were observed at a magnification of an optical microscope (OM: DMRM, LEICA). The different phases of the specimens were determined by X-ray diffraction analysis (XRD, PANalytical X'Pert Powder) and the corresponding phase composition of the alloy was analyzed by electron dispersive X-ray spectroscopy (EDX) attached to scanning electron microscopy (SEM ZEISS EVO18). The phase proportion was analyzed with statistic methods by using Image-Pro Plus image manipulation software.

Peer-reviewed version available at Metals 2018, 8, 407; doi:10.3390/met8060407

Firstly, the sample with σ phase was treated by electrolysis process in 10 wt % KOH aqueous solution in a voltage of 2 V, until the σ phase was completely dissolved. Then, the sample surface was rubbed up by alcohol and coated by the cyanoacrylate adhesive for insulating the residual sigma. After the cyanoacrylate glue completely solidified, the cotton swabs dipped in acetone were used to gently wipe the cyanoacrylate glue. Finally, the appropriate polishing processing is needed to make sure the surface smooth. The specific process can be shown in Fig. 1. It can be seen the σ phases was dissolved using this method and do not reach the second layer of sigma to expose them.

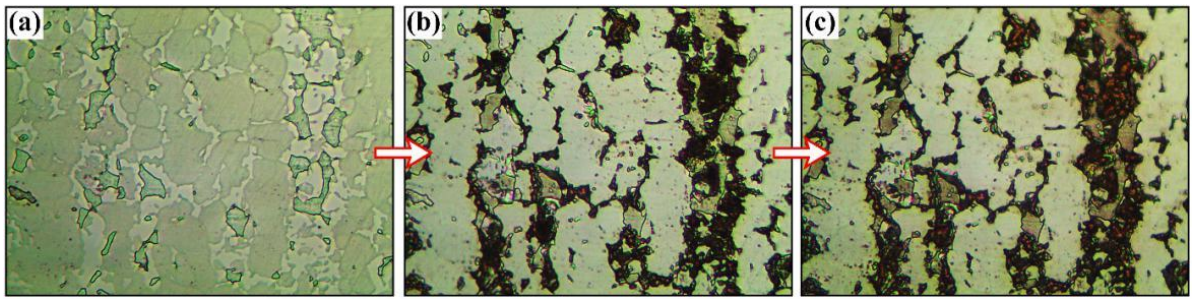


**Figure 1.** Process of preparing specimens without σ phase, (a) original specimen, (b) specimen electrolytically corroded by 10 wt % KOH, (c) specimen covered by cyanoacrylate glue

The electrochemical experiments were performed in 3.5 wt % NaCl solution, at room temperature and atmospheric pressure employing a three-electrode corrosion cell equipped with a saturated calomel electrode (SCE) reference electrode and a platinum foil counter electrode. The specimen with an exposure area of 1 $cm^2$ was used as a working electrode. Before the experiments, the samples were allowed to stabilize at an open circuit potential for 30 min, until the fluctuation potential within 10 mV. The polarization curves were recorded potentiodynamically at 0.5 mV $s^{-1}$, the potential scanning range from below 200 mV of open-circuit potentials to the potential when the current indicated that stable pitting had occurred.

## 3. Results

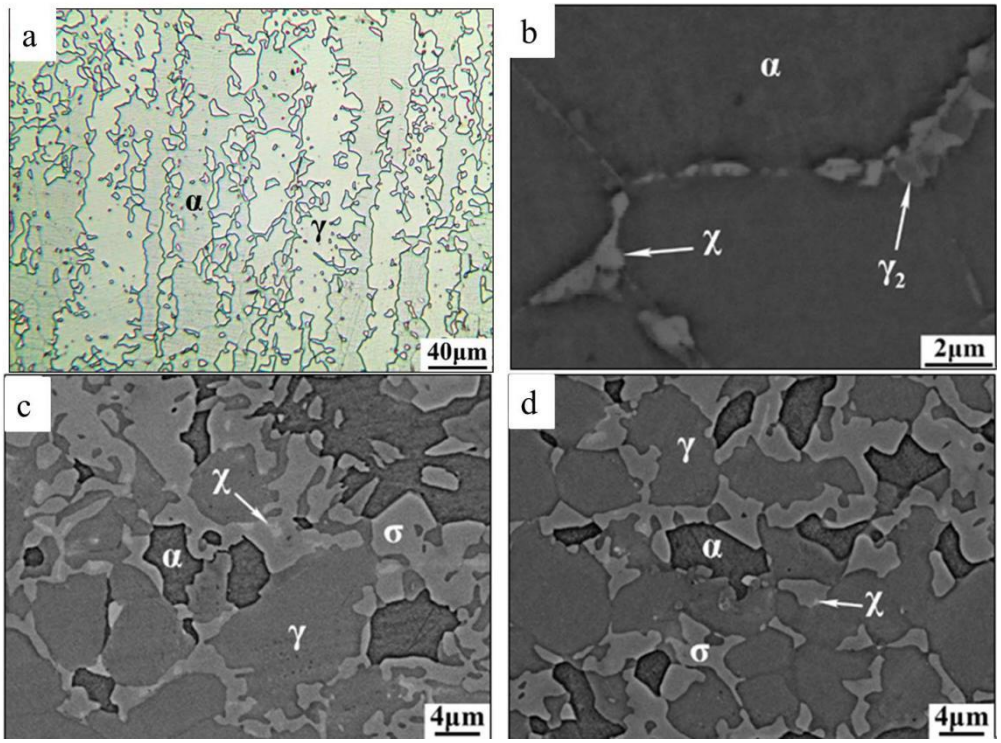

**Figure 2.** the SEM micrographs of hot-rolled 2205 duplex stainless steel after solid-solution treatment (a) and aging at 850°C for (b) 10 min, (c) 3 h and (d) 4 h

Fig. 2a shown the microstructure of the solution-annealed hot-rolled 2205 steels consists of elongated austenite islands in a ferrite matrix, and no obvious intermetallic phases were observed. During aging at 850℃for 10 min, χ phase preferentially nucleated at the boundary of ferrite and grew through the adjacent ferrite, as shown in Fig. 2b, which has been discussed in our previous work[29]. However, it can be observed form Fig.2c and Fig. 2d that with the increase of aging time to 3 and 4 h, the σ phase originated from the transformation of $\alpha \rightarrow \gamma 2+\sigma$ would gradually appear and coarse, where γ2 is the secondary austenite. Therefore, it can be considered that there was lots of σ phase in the matrix during aging for longer time. Besides that, a small amount of χ phase was also detected and distributed at the grains of σ phase.

Fig. 3 further showed the metallographic structure of 2205 duplex stainless steel with cold deformation after solid-solution and aging treatment. Fig.3a shown the microstructure of the solution-annealed cold-deformed specimen under optical microscope, and it can be seen that the austenitic phase with a lighter color is distributed in the ferrite phase, but the microstructure of cold-rolled samples become more elongated along the cold rolling direction, compare with the hot-rolled specimens. Meanwhile, the austenite grains of cold-deformed specimen are fine and not uniform, with a narrow strip shape, as a result of different local deformation. After aging for 10 min at 850°C, the bright white χ phase can also be observed in Fig. 3b. With prolonging the aged time to 3 h and 4 h, as shown in Fig. 3c and d, the σ phase precipitates began to appear at the boundary of ferrite and austenite phase, but its grain size is smaller than that of the hot rolled specimens. Fig. 3e and Fig. 3f further showed the EDS line-scan profile of cold-rolled specimen aging for 4 h, suggesting that the precipitated χ phase and σ phase have the enrichment of Cr and Mo elements, leading to the distribution of alloying elements such as Cr and Mo uneven in the matrix.

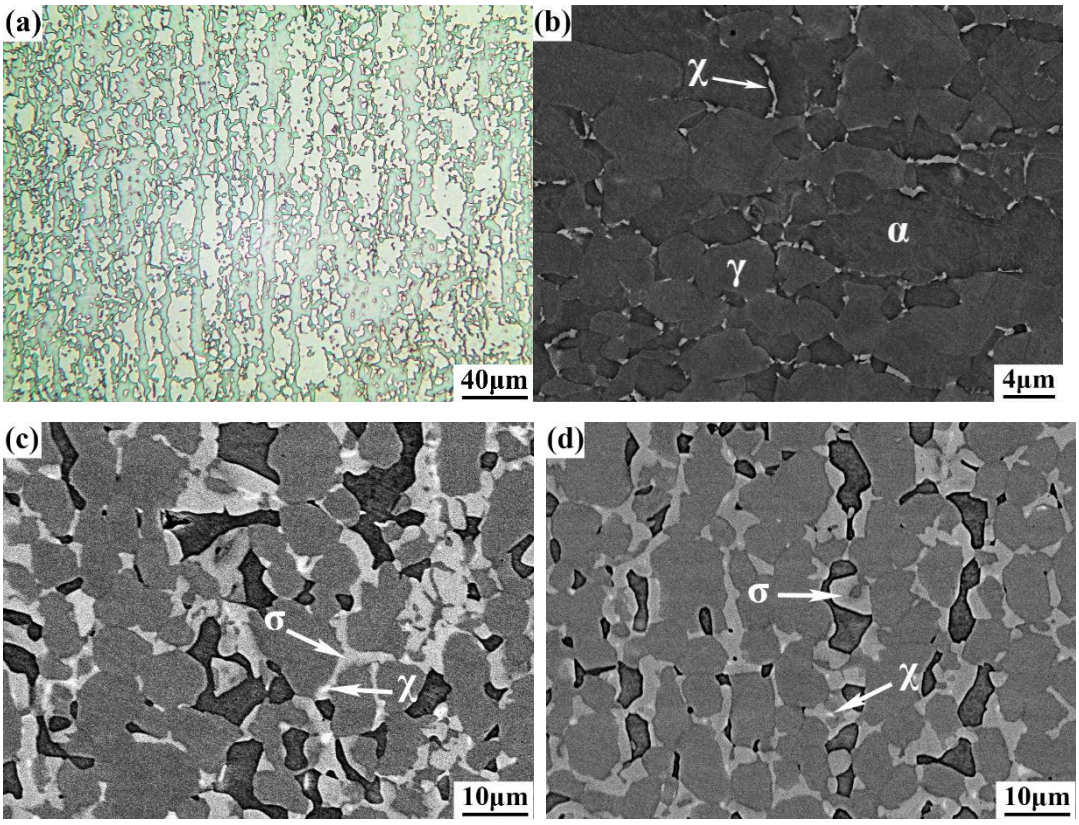

Preprints (www.preprints.org) | NOT PEER-REVIEWED | Posted: 16 April 2018 doi:10.20944/preprints201804.0200.v1

Peer-reviewed version available at Metals 2018, 8, 407; doi:10.3390/met8060407

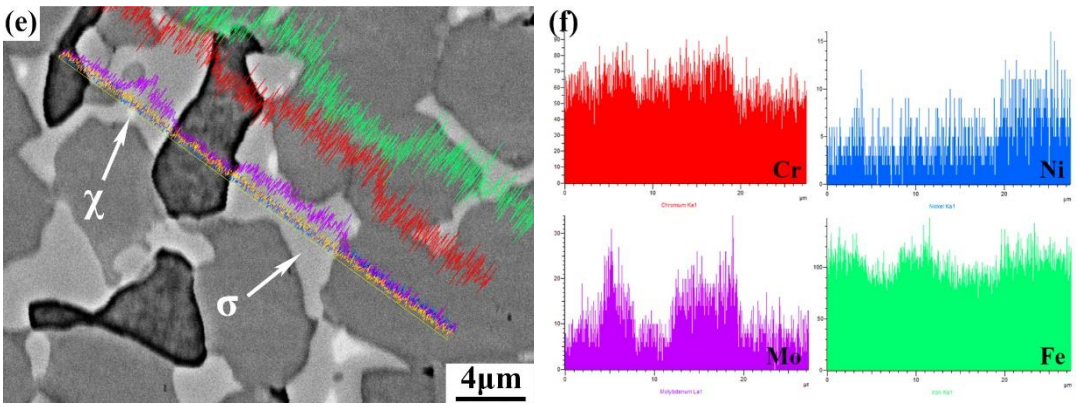


**Figure 3.** Microstructure of cold-rolled 2205 duplex stainless steel: (a) OM morphology of cold-rolled specimen, (b) SEM-BSE morphology of 10 min aged, (c) 3 h aged and (d) 4 h aged specimens at 850°C; (e) and (f) EDS line-scan profile of cold-rolled 4 h aged specimen

In Fig. 4 the σ phase volume fraction of the cold-rolled and hot-rolled 2205 steels is plotted as a function of aging time. As aging time prolongs, the amount of σ phase in the cold-rolled samples is gradually higher than that of the hot-rolled samples at the same aging time. In particular, the precipitations of the cold-rolled samples reach about 38.2 % for specimen aged at 850℃for 4 h, corresponding to 23.9 % in hot-rolled samples. The XRD diffraction spectra and local magnifications of cold-rolled and hot-rolled samples were further shown in the Fig. 5. It can be seen that the peak intensity of $\alpha$(110) relative to $\gamma$(111) decreased with the aging time, and sample aged for 4 h exhibited a small ferrite peak, indicating that a major fraction of the ferrite had been transformed into σ phase. The diffraction peak intensity of σ phase in cold-rolled material is significantly higher than that of hot rolled material when aging for 4 h, which suggests that more σ phase is precipitated in the cold-rolled specimen. Therefore, it can be confirmed that the precipitation of σ phase can be accelerated by the cold deformation in the subsequent aging process, which may be due to the increased defect and distortion energy during the cold-rolling process, promoting the transformation of the ferrite into σ phase. Combined the XRD and SEM results, the precipitated amounts and the size of σ phase in cold-rolled samples are much more and smaller than that of hot-rolled samples.

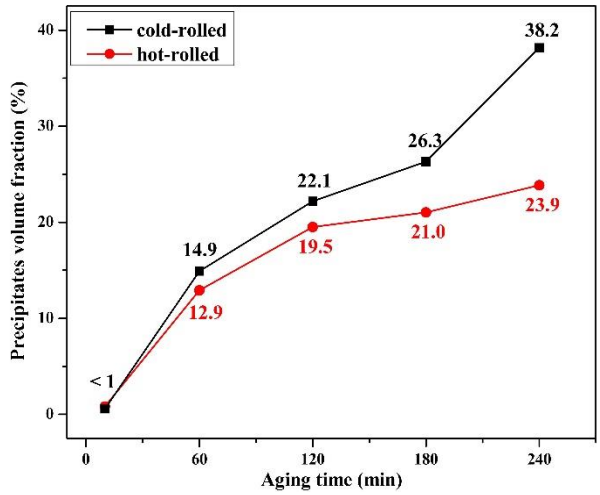


**Figure 4.** Changes in σ phase volume fraction of cold-rolled and hot-rolled of 2205 duplex stainless steel with prolonging aging time

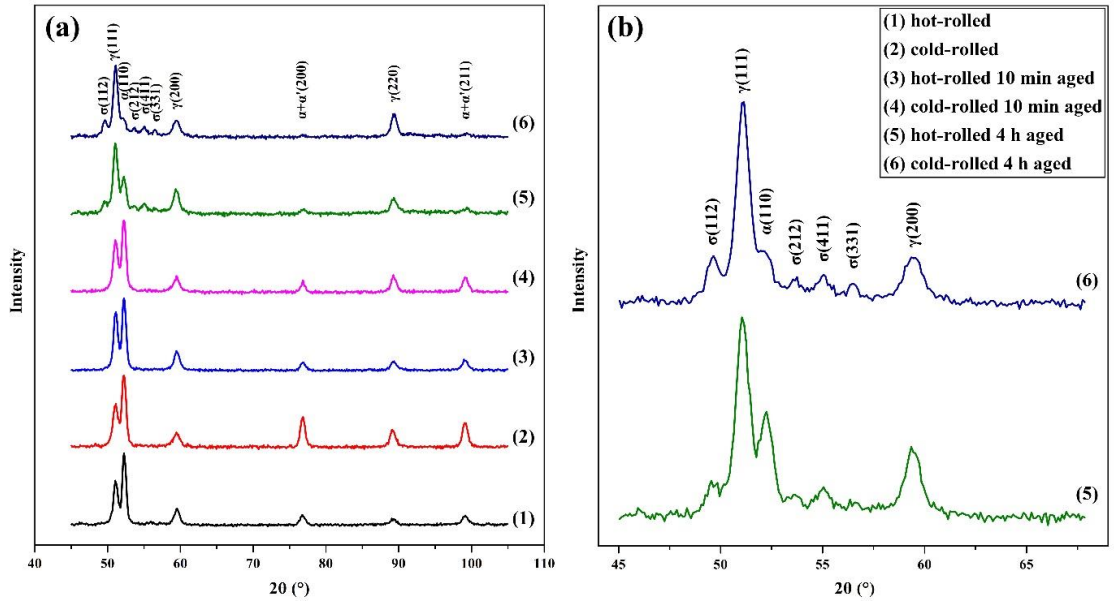


**Fig. 5.** Comparison of X-ray diffraction patterns between cold-rolled and hot-rolled 2205 duplex stainless steel without aging treatment, and after aging for 10 min, 4 h at 850°C, (a) overall patterns, (b) amplification patterns of cold-rolled and hot-rolled 4 h aged specimens

It can also be found from Fig. 5 that the peak intensity of the $\alpha$(200) and $\alpha$(211) in the cold-rolled solution-annealed samples is significantly higher than that of the hot-rolled samples, but the proportion of ferrite is not significantly increased by the metallographic analysis. In fact, it has been proved that the austenite phase in duplex stainless steel would be transformed into ε-martensite or $\alpha'$-martensite during cold deformation, and it can also be directly transformed into $\alpha'$-martensite when stacking fault energy is high[28]. Moreover, it is well known that both $\alpha'$-martensite and ferrite are body centered tetragonal crystal structure. Since the diffraction peak of $\alpha'$-martensite is consistent with the ferrite peak, the peak intensity of ferrite increase when containing $\alpha'$-martensite. Therefore, the XRD diffraction pattern of Fig. 5 indicates the formation of $\alpha'$-martensite in the cold rolling deformation. However, due to non-diffusive phase transition and unchanged chemical element of $\alpha'$-martensitic transformation, the direct observation of $\alpha'$-martensitic phase seems difficult.

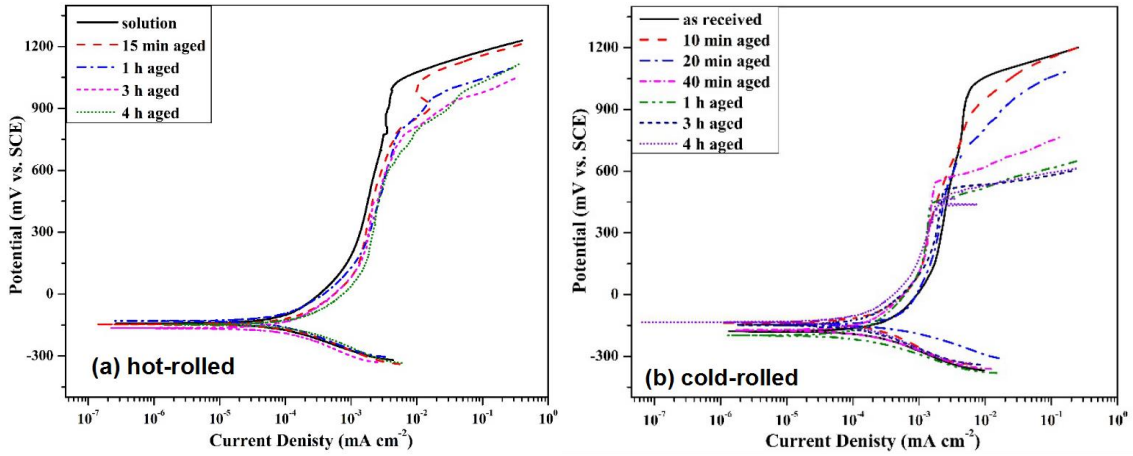


**Figure 6.** Comparison of potentiodynamic polarization curves between cold-rolled and hot-rolled 2205 duplex stainless steel after different aging treatment, (a) cold-rolled specimens, (b) hot-rolled specimens

**Table 2** $E_{pit}$ resulted from potentiodynamic polarization curves for hot-rolled 2205.

| hot-rolled | solid-sloution | 15 min | 1 h | 3 h | 4 h |
|---|---|---|---|---|---|
| $E_{pit}$ (mV, vs.SCE) | 1005 | 989 | 901 | 771 | 617 |

**Table 3** $E_{pit}$ resulted from potentiodynamic polarization curves for cold-rolled 2205

| cold-rolled | solid-sloution | 10 min | 20 min | 40 min | 1 h | 3 h | 4 h |
|---|---|---|---|---|---|---|---|
| $E_{pit}$ (mV, vs.SCE) | 1002 | 828 | 643 | 548 | 441 | 508 | 443 |

Fig. 6 shows the comparison of potentiodynamic polarization curves between cold-rolled and hot-rolled 2205 duplex stainless steel after different aging treatment in 3.5 wt % NaCl solution. Moreover, Table 2 and Table 3 compared the $E_{pit}$ resulte from potentiodynamic polarization curves for hot-rolled and cold-rolled 2205, respectively. It can be observed that the polarization curves of the hot-rolled and cold-rolled samples without aging treatment are similar, and both of the pitting potential ($E_{pit}$) are more than 1000 mV, indicating that the pitting resistance is largely consistent for the untreated cold-rolled and hot-rolled materials. However, for the cold-rolled sample, the $E_{pit}$ obviously decreased after aging only for 10 min. With prolonging aging time to 20 min, the $E_{pit}$ has been reduced to 643 mV, which is lower than the $E_{pit}$ of the hot-rolled specimens aging for 3 h. Further prolonging the aging time to 40 min, the $E_{pit}$ decreases to 548 mV, and the value is even lower than the hot-rolled samples aging for 4 h. When the aging time of cold-rolled sample extend to 1 h or even longer, the $E_{pit}$ further decreases and remains below 500 mV.

It is well-known that the corrosion resistance has always been considered in regard to the microstructure of materials. For the hot-rolled 2205 duplex stainless steel, the precipitation of σ phase gradually increases with prolonging aging time, and the corrosion resistance of the materials significantly decreases. In order to explain the correlation between microstructure and corrosion resistance, the corrosion morphology of hot-rolled 2205 duplex stainless steels aging for 10 min and 4 h, after potentiodynamic polarization, was characterized by SEM-BSE characterization and the EDS analysis, in which each residual phases are confirmed and presented in Table 4. As shown in Fig. 7a, it is observed that in the hot-rolled 2205 aged for shorter aging times, the pitting nucleation occurs preferably on grain boundaries or on ferrite/austenite interfaces. Combined with the Fig.7a and Table 4, the Cr content near precipitated phase or pitting is lower than that of ferrite, indicating that the pitting formation occurred in chromium-depleted areas associated to the precipitated phase. Further, a severe selective corrosion of the samples aged for 4 h mainly on sigma/ferrite interfaces is observed, as shown Fig. 7b. Since the σ phase has a relatively high Cr and Mo content, the pitting corrosion of hot-rolled 2205 steels preferred to take place around the σ phase is inevitable, and it tended to further grow by selective corrosion of chromium-depleted areas[30,31].

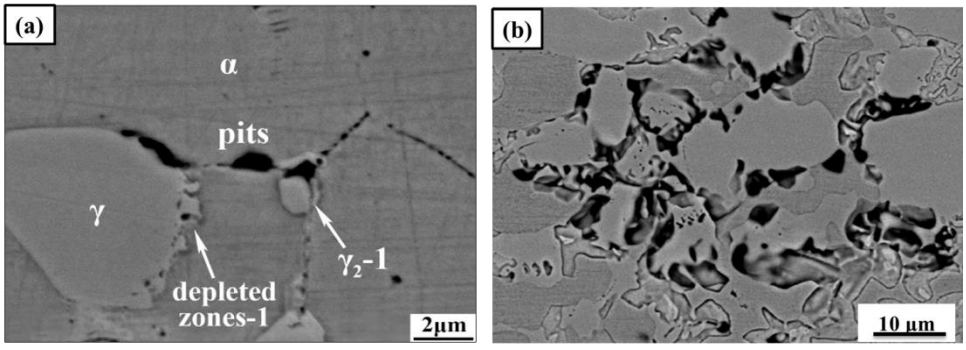

**Figure 7.** Corrosion morphology of hot-rolled 2205 duplex stainless steel after potentiodynamic polarization by SEM-BSE, (a) 10 min aged, (b) 4 h aged

**Table 4** Chemical composition of phases showed in Fig. 7(a) (wt. %)

| Position | Cr | Ni | Mo | Si | Mn | Fe |
|---|---|---|---|---|---|---|
| $\alpha$ | 24.73 | 3.53 | 4.57 | 0.75 | 1.50 | Bal. |
| $\gamma$ | 21.55 | 7.21 | 3.05 | 0.63 | 1.53 | Bal. |
| $\gamma$2-1 | 21.28 | 6.30 | 2.94 | 0.61 | 1.55 | Bal. |
| depleted zones-1 | 22.41 | 5.69 | 4.06 | 0.79 | 1.47 | Bal. |

Fig. 8 further showed corrosion morphology of cold-rolled 2205 duplex stainless steel aging for 10 min, 1 h and 4 h, after potentiodynamic polarization, by SEM-BSE. Fig. 8a shown the phase boundary of cold-rolled 2205 is preferred to be corroded in 3.5 wt % NaCl solution, and it is also worth noted that stripe pattern appear in the corrosion morphology of the sample aging 10 min, and the corresponding EDS analysis are shown in Table 5. The chemical composition of the stripe is the same as the surrounding austenite, which may be subject for $\alpha'$-martensite. Furthermore, as shown in Fig. 8b, c and d, the surface of cold-rolled 2205 still remains a large number of shallow white $\sigma$ phases after the corrosion and the selective corrosion focus on the sigma/ferrite interfaces. Therefore, different from the hot-rolled 2205 sample, the cold-rolled 2205 DSS after aging treatment was preferentially corroded from the phase boundary and $\alpha'$-martensite in 3.5 wt % NaCl solution, and the precipitates are basically not subject to be corroded in the initial process.

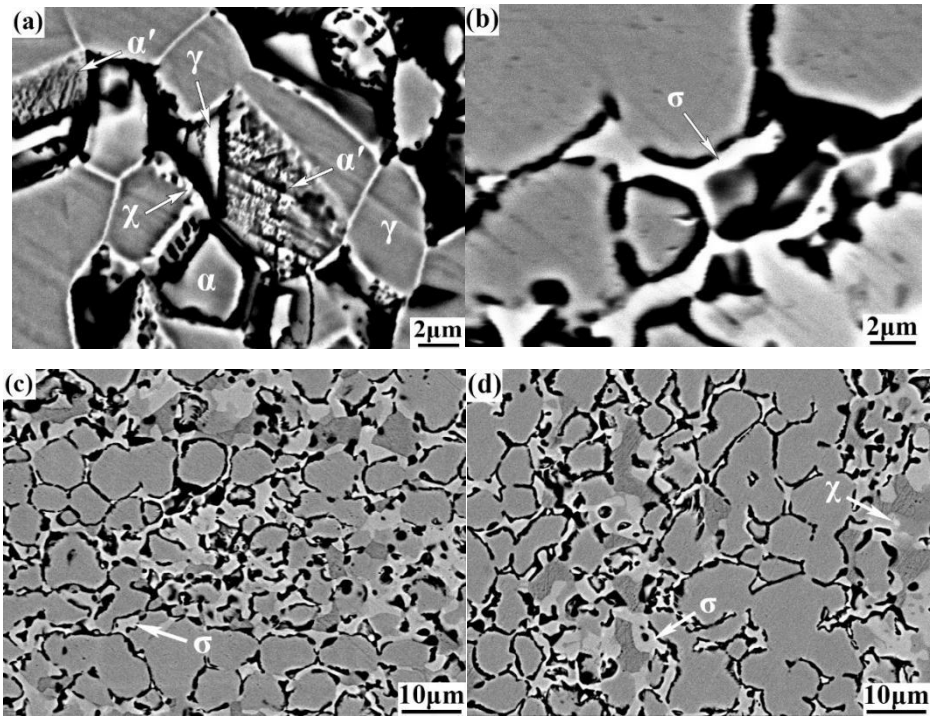


**Figure 8.** Corrosion morphology of cold-rolled 2205 duplex stainless steel after potentiodynamic polarization by SEM-BSE, (a) 10 min aged, (b) and (c) 1 h aged, (d) 4 h aged

Preprints (www.preprints.org) | NOT PEER-REVIEWED | Posted: 16 April 2018 doi:10.20944/preprints201804.0200.v1

Peer-reviewed version available at Metals 2018, 8, 407; doi:10.3390/met8060407

**Table 5** Chemical composition of strain-induced martensite and γ phase showed in Fig. 8(a) (wt. %)

| position | Cr | Ni | Mo | Si | Mn | Fe |
|---|---|---|---|---|---|---|
| α′ | 21.27 | 6.37 | 3.31 | 0.75 | 1.57 | Bal. |
| γ | 21.43 | 6.22 | 2.92 | 0.64 | 1.79 | Bal. |

## 4. Discussion

To investigate in detail the corrosion behavior of hot-rolled and cold-rolled 2205 DSS, the σ phase is selectively dissolved for fabricating the specimens without σ phase by electrochemical method. The potentiodynamic polarization curves between original specimens and specimens without σ phase were further shown in Fig. 9. For the hot-rolled materials, the $E_{pit}$ of sample removing σ phase would rise to that of solution-annealed alloys. Therefore, the precipitated σ phase is the main factors affecting the corrosion resistance of the hot-rolled material, which may be descried to the formation of Cr-depleted zone around σ phase, and preferred to selectively corrosion. When σ phase is removed, the corrosion resistance of the materials would be obviously restored, which suggests the chromium redistribution in the matrix of hot-rolled 2205.

For the cold-rolled 2205 DSS, the precipitation content of σ phase was increased, and the precipitation speed of precipitates was also accelerated. This seems to undermine the corrosion resistance of cold-rolled 2205 DSS, compared with the hot-rolled materials. However, even if the σ phase was eliminated from cold-working materials, its $E_{pit}$ only increase from 443 mV to 630 mV, still much lower than that of non-aging sample (1002 mV). This suggests more complicated influence factor on the corrosion resistance of cold-rolled materials. Besides the effect of σ phase on the corrosion resistance, on the one hand, the cold-deformation of 2205 DSS easily generated the dislocation, deformation twinning and dislocation-twin interactions, where the nucleation of the pitting attack is much more likely to happen. Moreover, a more defective passive film on the cold-rolled 2205 DSS is likely formed in the defects of the grains, and imperfect oxides grown in the bulk of the material, which can be proved from the Fig. 8. On the other hand, the strain-induced martensite in cold-worked 2205 may be active than other precipitate phase and matrix phase, so it was also easily corroded in the early stage, which is similar to the reported role of strain-induced martensite in cold-work 304 steels[32]. Further research needs to be done to clarify the influence factor of the corrosion resistance for the cold-rolled 2205 DSS.

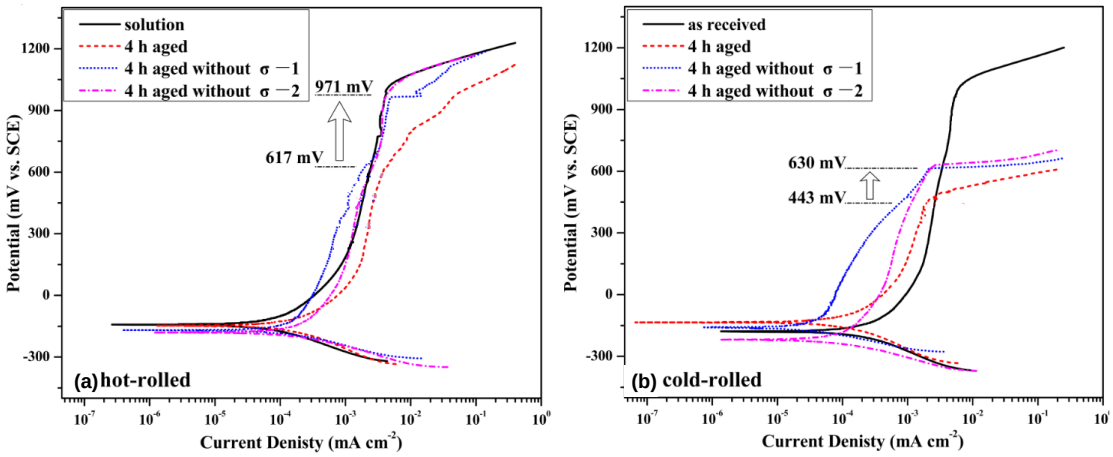


**Figure 9.** Comparison of potentiodynamic polarization curves between original specimens and specimens without σ phase, (a) hot-rolled specimens, (b) cold-rolled specimens

## 5. Conclusions

The difference of precipitates-induced selective corrosion in hot-rolled and cold-rolled 2205 duplex stainless steel was evaluated by microstructural analyses of the sample aging at 850°C for different times combined with electrochemical methods. The Chi phase and Sigma phase was precipitated in turn after aging treatment of hot-rolled and cold-rolled materials, but the precipitate rate in cold rolled material is faster, resulting from the stored internal energy and increased defect density. The precipitated amount of sigma phase in cold-rolled materials is more than that of hot-rolled material under the same aging condition. Meanwhile, the strain-induced martensite structure was also produced by the transformation of austenite under the condition of cold deformation.

The corrosion resistance of the solution-annealed cold-rolled material is similar to the hot-rolled material, but the corrosion resistance of cold-rolled material is weaker than that of hot-rolled material after aging treatment. Pitting nucleates preferentially in the Cr-depleted region around σ phase for the hot-rolled 2205 aged specimen, and the corrosion resistance of hot-rolled 2205 removing σ phase recover to close to the level of solution-annealed 2205. However, not only the σ phase but also the strain-induced martensite and defects which were induced by cold deformation have an important influence on the corrosion resistance of cold-rolled 2205 DSS. Correspondingly, the initiation of pitting corrosion takes place at the phase boundary, defect and martensite for the cold-rolled 2205 aged specimen, leading to a lower corrosion resistance, compared with hot-rolled 2205.

**Acknowledgments:** This research was supported by the National Natural Science Foundation of China (Grant No. 51371123) and Shanxi Province Science Foundation for Youths (201601D202033).

**Author Contributions:** Tao Gao performed research, analyzed the data and wrote the paper; Qi Sun helped in the experimental part; Jian wang and Peide Han assisted in the data analysis and revised manuscript

**Conflicts of Interest:** The authors declare no conflict of interest

## References

1. Pohl, M.; Storz, O.; Glogowski, T. Effect of intermetallic precipitations on the properties of duplex stainless steel. *Mater. Charact.* **2007**, *58*, 65-71. DOI:10.1016/j.matchar.2006.03.015

2. Sato, Y.S.; Nelson, T.W.; Sterling, C.J. ; Steel, R.J.; Pettersson, C.-O. Microstructure and mechanical properties of friction stir welded SAF 2507 super duplex stainless steel. *Mat. Sci. Eng. A.* **2005**, *397*,376-384. DOI: 10.1016/j.msea.2005.02.054

3. Wang, H. Investigation of a Duplex Stainless Steel as Polymer Electrolyte Membrane Fuel Cell Bipolar Plate Material. *J. Electrochem. Soc.* **2005,** *152*, B99-B104. DOI: 10.1149/1.1854612.

4. Charles, J.; Duplex stainless steels, a review after DSS'07 in Grado. *Rev. Metall.* **2008**,*105*, 455-465. DOI:10.1051/metal:2008028

5. Ghosh, S.K.; Mondal, S. Effect of heat treatment on microstructure and mechanical properties of duplex stainless steel. T. *Indian I. Metals.* **2008**, *61*, 33-37. DOI: 10.1007/s12666-008-0062-x

6. Liu, J.M.; Liu, J; Fan, G.W.; Du, D.F.; Li, G.P.; Chai, C.J. Effect of Solution Treatment on Microstructure and Properties of the SAF2507 Super Duplex Stainless Steel. *Mater. Sci. Forum.* **2012**, *724*, 3-6. DOI: 10.4028/www.scientific.net/MSF.724.3

7. Naghizadeh, M.; Moayed, M.H. Investigation of the effect of solution annealing temperature on critical pitting temperature of 2205 duplex stainless steel by measuring pit solution chemistry. *Corros. Sci.* **2015**, *94*, 179-189. DOI: 10.1016/j.corsci.2015.01.051

8. Lacerda, J.C.D.; Cândido, L.C.; Godefroid, L,B. Corrosion behavior of UNS S31803 steel with changes in the volume fraction of ferrite and the presence of chromium nitride. *Mat. Sci. Eng. A.* **2015**, *648*, 428-435. DOI: 10.1016/j.msea.2015.09.092

9. Cheng, X.Q.; Li, X.G.; Dong, C.F. Study on the passive film formed on 2205 stainless steel in acetic acid by AAS and XPS. *Int. J. Min. Met. Mater.* **2009**,*16*,170-176. DOI: 10.1016/S1674-4799(09)60029-7

10. Luo, H.; Dong, C.F.; Xiao, K.; Li, X.G. Characterization of passive film on 2205 duplex stainless steel in sodium thiosulphate solution. *Appl. Sur. Sci.* **2011,** *258*, 631-639. DOI: 10.1016/j.apsusc.2011.06.077

11. Lv, J.; Liang, T.; Wang, C.; Dong, L. Comparison of corrosion properties of passive films formed on coarse grained and ultrafine grained AISI 2205 duplex stainless steels. *J. Electrochem. Soc.* **2015**, *757*, 263-269. DOI: 10.1016/j.jelechem.2015.09.036

12. Lv, J.; Liang, T.; Wang, C.; Guo, T. Influence of sensitization on passive films in AISI 2205 duplex stainless steel. *J. Alloy. Compd.* **2016**, *658*, 657-662.

13. Deng, B.; Wang, Z.; Jiang, Y.; Wang, H.; Gao, J.; Li, J. Evaluation of localized corrosion in duplex stainless steel aged at 850°C with critical pitting temperature measurement. *Electrochi. Acta.* **2009**, *54*, 2790-2794. DOI: 10.1016/j.electacta.2008.11.038

14. Hoseinpoor, M.; Momeni, M.; Moayed, M.H.; Davoodi, A. EIS assessment of critical pitting temperature of 2205 duplex stainless steel in acidified ferric chloride solution. *Corros. Sci.* **2014**, *80*, 197–204. DOI: 10.1016/j.corsci.2013.11.023

15. Chan,K.; Tjong, S. Effect of Secondary Phase Precipitation on the Corrosion Behavior of Duplex Stainless Steels. *Materials*. **2014**, *7*, 5268-5304. DOI: 10.3390/ma7075268

16. Huang, C.S.; Shih, C.C. Effects of nitrogen and high temperature aging on σ phase precipitation of duplex stainless steel. *Mat. Sci. Eng. A.* **2005**, *402*, 66-75. DOI: 10.1016/j.msea.2005.03.111

17. Santos, D.C.D.; Magnabosco, R.; Moura-Neto, C.D. Influence of sigma phase formation on pitting corrosion of an aged uns s31803 duplex stainless steel. *Corrosion*. **2013**, 69, 900-911. DOI: 10.5006/0768

18. Park, C.J.; Rao, V.S.; Kwon, H.S. Effects of sigma phase on the initiation and propagation of pitting corrosion of duplex stainless steel. *Corrosion*., **2005**, *61*, 76-83. DOI: 10.5006/1.3278163

19. Pohl, M.; Storz, O.; Glogowski, T. σ-phase morphologies and their effect on mechanical properties of duplex stainless steels. *Int. J. Mater. Res.* **2008**, 99, 1163-1170. DOI: 10.3139/146.101738

20. Chen, T.H.; Weng, K.L.; Yang, J.R. The effect of high-temperature exposure on the microstructural stability and toughness property in a 2205 duplex stainless steel. *Mat. Sci. Eng. A.* **2002**, *338*, 259-270. DOI: 10.1016/S0921-5093(02)00093-X

21. Elmer, J.W.; Palmer, T.A.; Specht, E.D. In situ observations of sigma phase dissolution in 2205 duplex stainless steel using synchrotron X-ray diffraction. *Mat. Sci. Eng. A.* **2007**, *459*, 151-155. DOI: 10.1016/j.msea.2007.01.071

22. Sieurin, H.; Sandström, R. Sigma phase precipitation in duplex stainless steel 2205. *Mat. Sci. Eng. A.* **2007**, *444*, 271-276. DOI: 10.1016/j.msea.2006.08.107

23. Lai, J.K.L.; Wong, K.W.; Li, D.J. Effect of solution treatment on the transformation behaviour of cold-rolled duplex stainless steels. *Mat. Sci. Eng. A.* **1995**, 203, 356-364. DOI: 10.1016/0921-5093(95)09863-1

24. Neissi, R.; Shamanian, M.; Hajihashemi, M. The Effect of constant and pulsed current gas tungsten arc welding on joint properties of 2205 duplex stainless steel to 316L Austenitic Stainless Steel. *J. Mater. Eng. Perform.* **2016**, *25*, 2017-2028. DOI: 10.1007/s11665-016-2033-4

25. Yurtisik, K.; Tirkes, S. Fatigue Cracking of hybrid plasma gas metal arc welded 2205 duplex stainless steel. *Materialprufung*, **2014**, *56*, 800-805. DOI: 10.3139/120.110643

26. Örnek, C.; Engelberg, D.L. Towards understanding the effect of deformation mode on stress corrosion cracking susceptibility of grade 2205 duplex stainless steel. *Mat. Sci. Eng. A.* **2016**, *666*, 269-279. DOI: 10.1016/j.msea.2016.04.062

27. Cho, H.S.; Lee, K. Effect of cold working and isothermal aging on the precipitation of sigma phase in 2205 duplex stainless steel. *Mater. Charact.* **2013**, *75*, 29-34. DOI: 10.1016/j.matchar.2012.10.006

28. Breda, M.; Brunelli, K.; Grazzi F. Effects of Cold Rolling and Strain-Induced Martensite Formation in a SAF 2205 Duplex Stainless Steel. *Metall. Mater. Tran. A.* **2015**, *46*,577-586. DOI: 10.1007/s11661-014-2646-x

29. Sun, Q.; Wang, J.; Li, H.B.; Hu, Y.D.; Bai, J.G.; Han, P.D. Chi Phase after Short-term Aging and Corrosion Behavior in 2205 Duplex Stainless Steel. *J. Iron Steel Res. Int.* **2016**, *23*, 1071-1079. DOI : 10.1016/S1006-706X(16)30159-5

30. Magnabosco, R. Alonso-Falleiros, N. Sigma Phase Formation and Polarization Response of UNS S31803 in Sulfuric Acid. *Corrosion.* **2005**, *61*, 807-814. DOI: 10.5006/1.3278215

31. Warren, A.D.; Harniman, R.L.; Guo, Z.; Younes, C.M.; Flewitt, P.E.J.; Scott, T.B. Quantification of sigma-phase evolution in thermally aged 2205 duplex stainless steel. *J. Mater. Sci.* **2016**, *51*, 694-707. DOI: 10.1007/s10853-015-9131-9

32. Xu, C.; Gang, H. Effect of deformation-induced martensite on the pit propagation behavior of 304 stainless steel. *Anti-Corros. Method. M.* **2004**, 51,381-388. DOI: 10.1108/00035590410560921